The Binding of DYNLL2 to Myosin Va Requires Alternatively Spliced Exon B and Stabilizes a Portion of the Myosin's Coiled-Coil Domain†

Wolfgang Wagner,‡ Elfrieda Fodor,§ Ann Ginsburg,§ and John A. Hammer, III*,‡

Laboratory of Cell Biology and Laboratory of Biochemistry, National Heart, Lung, and Blood Institute, National Institutes of Health, Bethesda, Maryland 20892

Received June 8, 2006; Revised Manuscript Received July 31, 2006

ABSTRACT: The myosin Va light chain DYNLL2 has been proposed to function as an adaptor to link the myosin to certain cargo. Here, we mapped the binding site for DYNLL2 within the myosin Va heavy chain. Copurification and pull-down experiments showed that the heavy chain contains a single DYNLL2 binding site and that this site resides within a discontinuity in the myosin's central coiled-coil domain. Importantly, exon B, an alternatively spliced, three-amino acid exon, is a part of this binding site, and we show in the context of full-length myosin Va that this exon is required for DYNLL2−myosin Va interaction. We investigated the effect of DYNLL2 binding on the structure of a myosin Va heavy chain fragment that contains the DYNLL2 binding site and flanking sequence, only parts of which are strongly predicted to form a coiled coil. Circular dichroism measurements revealed a DYNLL2-induced change in the secondary structure of this dimeric myosin fragment that is consistent with an increase in α-helical coiled-coil content. Moreover, the binding of DYNLL2 considerably stabilizes this heavy chain fragment against thermal denaturation. Analytical ultracentrifugation yielded an apparent association constant of $\sim 3 \times 10^6$ M^{-1} for the interaction of DYNLL2 with the dimeric myosin fragment. Together, these data show that alternative splicing of the myosin Va heavy chain controls DYNLL2−myosin Va interaction and that DYNLL2 binding alters the structure of a portion of the myosin's coiled-coil domain. These results suggest that exon B could have a significant impact on the conformation and regulatory folding of native myosin Va, as well as on its interaction with certain cargos.

Mouse myosin Va is an actin-based motor protein that is capable of walking processively along actin filaments and that functions in the transport of membrane-bound organelles (*1*−*3*). The myosin consists of two identical heavy chains and as many as 12 calmodulin light chains (although polypeptides resembling conventional myosin light chains may substitute for some of the calmodulins in certain myosin V homologues). The N-terminal approximately half of the myosin Va heavy chain is composed of a motor domain followed by six IQ motifs that serve as the binding sites for calmodulin or related light chains. The remainder of the heavy chain consists of a central α-helical coiled-coil stalk domain that mediates heavy chain dimerization followed by a C-terminal globular tail domain that has been implicated in cargo attachment (*1*, *4*). Alternative splicing of three exons (exons B, D, and F), all of which are inserted at sites in the central stalk domain where the coiled-coil structure is predicted to be disrupted (*5*), conveys at least in part cell type-specific functions on myosin Va. For example, the myosin Va isoform responsible for melanosome transport in melanocytes, which contains exons D and F but lacks exon B, requires exon F for its interaction with melanosomes (*6*). Interestingly, the myosin Va isoform that is widely expressed in brain lacks exons D and F but contains exon B (*5*). The specific function of exon B, which consists of only three amino acid residues (DDK), is unknown.

Unlike other myosins characterized to date, myosin Va purified from chicken and mouse brain also contains an ∼10 kDa protein of the dynein light chain LC8 (DYNLL)[1] family (*7*−*9*). As the name implies, DYNLL proteins were originally identified as light chains for the microtubule-based motor protein dynein (*7*, *10*−*12*). DYNLL proteins have been

† This work was supported by the Intramural Research Program of the National Institutes of Health, National Heart, Lung, and Blood Institute.

* To whom correspondence should be addressed: National Heart, Lung, and Blood Institute, National Institutes of Health, Building 50, Room 2523, 9000 Rockville Pike, Bethesda, MD 20892-8017. Telephone: (301) 496-8960. Fax: (301) 402-1519. E-mail: hammerj@nhlbi.nih.gov.

‡ Laboratory of Cell Biology.

§ Laboratory of Biochemistry.

[1] Abbreviations: Bim, Bcl-2 interacting mediator of cell death; Bmf, Bcl-2-modifying factor; br, brain-spliced isoform of the myosin Va heavy chain; CD, circular dichroism; DTT, dithiothreitol; DYNC1I1, cytoplasmic dynein 1 intermediate chain 1; DYNLL, dynein light chain LC8; EDC, 1-ethyl-3-[3-(dimethylamino)propyl]carbodiimide hydrochloride; GKAP, guanylate kinase-associated protein (also known as SAPAP, synapse-associated protein 90 associated protein, or DAP1α, discs-large-associated protein); GST, glutathione *S*-transferase; His tag, six-histidine tag; IPTG, isopropyl β-D-thiogalactopyranoside; mc, melanocyte-spliced isoform of the myosin Va heavy chain; MyoVa$^{1194-1316}$, fragment corresponding to residues 1194−1316 of the brain myosin Va heavy chain containing the DYNLL2 binding site; MyoVa$^{1194-1316}$ΔExonB, like MyoVa$^{1194-1316}$ but lacking the three residues of exon B (DDK); Ni−NTA, nickel−nitrilotriacetic acid; nNOS, neuronal nitric oxide synthase; ORF, open reading frame; PBS, phosphate-buffered saline; PCR, polymerase chain reaction; S-NHS, *N*-hydroxysulfosuccinimide; SDS−PAGE, sodium dodecyl sulfate−polyacrylamide gel electrophoresis; TEV, tobacco etch virus.

10.1021/bi061142u
Published on Web 09/02/2006

highly conserved throughout evolution (>94% sequence identity between *Drosophila melanogaster* and mammalian orthologs) (*13*). Mammals express two closely related isoforms: DYNLL1 (formerly called dynein LC8a, DLC1, or PIN) and DYNLL2 (formerly called dynein LC8b or DLC2), which is 93% identical to DYNLL1 (*12*−*16*). Microsequencing of the DYNLL isoform that is copurified with chicken brain myosin Va (*8*), analyses of myosin Va purified from mouse spleen and chicken brain using a DYNLL1-specific antibody (*17*), and analysis of myosin Va purified from cells overexpressing tagged versions of DYNLL1 and DYNLL2 (*18*) all argue that only DYNLL2 acts as a light chain for myosin Va, although both DYNLL isoforms interact with myosin Va tail fragments robustly in yeast two-hybrid assays and myosin Va binds equally well to recombinant DYNLL1 and DYNLL2 (*16*).

Numerous targets for DYNLL other than dynein and myosin Va have been identified, including neuronal nitric oxide synthase (nNOS) (*14*), the postsynaptic scaffolding proteins gephyrin and GKAP (*16*, *19*−*21*), the pro-apoptotic proteins Bim and Bmf (*17*, *22*), and swallow and egalitarian, two proteins required for mRNA localization in *Drosophila* (*23*, *24*). The identification of the DYNLL binding site in a number of these proteins has led to the formulation of two distinct consensus sequences for binding DYNLL: (1) G(I/V)QVD, which is present for example in nNOS and GKAP, and (2) (K/R)XTQT (X is any amino acid), which is present for example in swallow, Bim, Bmf, and intermediate chain 1 (DYNC1I1) of cytoplasmic dynein 1 (*25*−*28*).

Physical and structural analyses have shown that DYNLL exists under physiological conditions as a dimer, including when bound to dynein and myosin Va (*7*, *26*, *28*−*31*). Moreover, crystal and NMR structures of DYNLL in a complex with target peptides have shown that the DYNLL homodimer possesses two identical target binding grooves on opposite faces of the dimer and that the peptides bound to each face are oriented parallel to each other (*18*, *26*, *28*, *32*). Strikingly, both types of target peptide, one from nNOS and one from Bim, bind to DYNLL in an essentially identical manner wherein they assume a β-strand conformation that is antiparallel to a β-strand in DYNLL (*26*, *28*). In both cases, the glutamine in the target peptide [i.e., G(I/V)**Q**VD and (K/R)XT**Q**T] makes hydrogen bonds with residues Glu35 and Lys36 at the start of helix α2 of DYNLL (*26*, *28*). The importance of this glutamine residue for DYNLL binding has been demonstrated by mutational studies (*18*, *27*, *33*). Notably, a sequence that conforms to either of these two DYNLL recognition consensus motifs (including the highly conserved glutamine) does not exist in the myosin Va heavy chain.

Initial efforts to identify the DYNLL binding site in myosin Va employed protease digestion of tissue-purified chicken brain myosin Va (*8*). This study showed that DYNLL associates with an ~80 kDa C-terminal fragment of the myosin that contains much of its central coiled-coil stalk domain and all of its globular tail domain. Consistent with this, yeast two-hybrid analyses and pull-down experiments revealed the presence of a DYNLL binding site in a fragment of the brain-spliced isoform of mouse myosin Va that spans residues 1236−1420, which corresponds to a C-terminal portion of the stalk domain (*16*).

In a more general effort to identify and characterize binding sites for DYNLL1, Lajoix et al. (*33*) probed arrays of peptides immobilized on cellulose membranes for their ability to bind DYNLL1. Extensive mutational analyses of the peptides that bound DYNLL1 led to the definition of a refined, loosely conserved, seven-residue DYNLL1-binding consensus motif (DKXTQTD) where the glutamine at position 5 is the most conserved residue, being present in 18 of 19 target peptides. Surprisingly, Lajoix et al. (*33*) also identified peptides from chicken brain myosin Va that bind to DYNLL1. A minimal myosin Va peptide that was able to bind to DYNLL1 was EDKNTMTD, which corresponds to residues 1286−1293 in chicken brain myosin Va, and is homologous to residues 1284−1291 in mouse brain myosin Va. Although this peptide resembles the DKXTQTD consensus identified in their peptide array screen, the highly conserved glutamine is replaced with a methionine in the myosin Va peptide (*33*). Mutational analyses of this myosin Va peptide revealed that five residues (those shown in bold; E**D**KN**TMTD**) are crucial for binding DYNLL1 and indicated that changing the methionine at position 6 to a glutamine increases the affinity of the peptide for DYNLL1 (*33*). While these studies point to residues 1284−1291 in mouse myosin Va as a possible binding site for DYNLL, they do not show that this sequence binds DYNLL2, the isoform that appears to serve as the myosin Va light chain in vivo, nor do they show that this sequence serves as the binding site for DYNLL2 in the context of native, full-length myosin Va. Moreover, it is not clear from their work if there is more than one DYNLL binding site within the myosin Va heavy chain.

The pro-apoptotic protein Bmf, as well as the postsynaptic scaffolding protein GKAP, has been shown to interact with myosin Va. Given that all three of these proteins interact with DYNLL2 and that the DYNLL2 homodimer possesses two identical surfaces for binding target proteins, it has been proposed that DYNLL2 serves to link Bmf and GKAP to myosin Va by binding to both proteins simultaneously (*16*, *17*). Similarly, Bim is thought to associate with dynein via their shared interaction with DYNLL1 (*22*), and a *Drosophila* DYNLL isoform has been proposed to bridge the interaction between dynein and the swallow protein by binding to both proteins simultaneously (*23*). These and other studies (*21*, *24*, *34*) suggest that one general function of DYNLL proteins may be to link motor proteins and their cargo.

While DYNLL proteins may well serve as cargo adaptors, the fact remains that many DYNLL target proteins are themselves homodimeric molecules. This fact raises the possibility that a single DYNLL homodimer may in some if not most cases bind simultaneously to identical DYNLL binding sites in its homodimeric target (e.g., each of the two identical heavy chains in native myosin Va, each of the two identical ~74 kDa polypeptides that comprise DYNC1I1). Such an interaction could serve to alter and/or stabilize a particular conformation in the target protein. Consistent with this idea, the binding of DYNLL to an unstructured segment within the *Drosophila* homologue of DYNC1I alters the conformation of the intermediate chain, inducing the formation of α-helical structure in that segment (*35*). Similarly, the interaction of DYNLL with the swallow protein favors the assembly in swallow of a stable, dimeric α-helical coiled

coil located immediately N-terminal of its DYNLL binding site (*36*).

In this study, we show that the myosin Va heavy chain contains a single binding site for DYNLL2 and that exon B, an alternatively spliced exon present in the brain-spliced isoform of myosin Va, constitutes an essential part of this binding site. Moreover, our data demonstrate that DYNLL2 binding alters the conformation of a portion of the myosin's coiled-coil domain, causing an increase in local α-helical coiled-coil content and thermal stability. These results expand our knowledge of the functional consequences of alternative splicing of the myosin Va heavy chain mRNA.

MATERIALS AND METHODS

Plasmids. The construction of the baculovirus vectors for expression in Sf9 insect cells of full-length, FLAG-tagged mouse myosin Va [brain-spliced isoform (br), melanocyte-spliced isoform (mc), and mc myosin Va lacking exon D or F] was described previously (*37*). To create vectors expressing br myosin Va lacking exon B and mc myosin Va containing exon B, an ~2.5 kb *Bgl*II fragment that includes the alternatively spliced region of myosin Va was released from the br and mc myosin Va vectors, blunt-ended by Klenow fill-in, and ligated with *Sal*I-digested pBluescript SK+ that had been blunt-ended by Klenow fill-in. Exon B was then removed or introduced using a QuikChange II SDM kit (Stratagene) and the following oligonucleotides: CCAAAAAGAAGCCATCCAACCCAAGGATGACAAGAATACAATGACAGATTCCAC (for deletion of exon B) and CCAAAAAGAAGCCATCCAACCCAAGAATACAATGACAGATTCCACAATTC (for insertion of exon B), along with their reverse complements. The modified *Bgl*II fragment was then released from these plasmids and used to replace the corresponding *Bgl*II fragment in full-length, FLAG-tagged br or mc myosin Va cDNAs present in Bluescript (*37*), thereby generating br myosin Va lacking exon B and mc myosin Va containing exon B. These FLAG-myosin Va cDNAs were released by *Not*I digestion and ligated with *Not*I-digested pVL1392 (Invitrogen). A similar strategy was used to create a baculovirus vector expressing br myosin Va lacking residues 1316−1319 (KETN), except that these residues were deleted using the following oligonucleotide and its reverse complement: GGTGAAATAGCACAAGCATATATTGGTTTGAGGCTCTTAGAATCCCAGCTACAG. The baculovirus vector for the expression of HA-tagged DYNLL2 was created by ligating *Eco*RI- and *Bam*HI-digested pVL1392 with an *Eco*RI- and *Bam*HI-digested PCR fragment containing the mouse *Dynll2* open reading frame (ORF) amplified from plasmid DLC8B-pCMVsport using primers CTAGAATTCGCCACCATGGCTTACCCATACGACGTCCCAGACTACGCTTCTGACCGGAAGGCAGTGATCAAGAACGC and ACTGGATCCCTAGCCCGACTTGAAGAGGAGGATTGCAACTTGACC. The baculovirus vector for the expression of myc-tagged DYNLL1 was created by ligating *Eco*RI- and *Bam*HI-digested pVL1392 with an *Eco*RI- and *Bam*HI-digested PCR fragment containing the mouse *Dynll1* ORF amplified from plasmid DLC8A using primers CTAGAATTCGCCACCATGGAGCAAAAGCTCATTTCTGAAGAGGACCTGTGCGACCGGAAGGCGGTGATCAAAAATGC and CATGGATCCTTAACCAGATTTGAACAGAAGAATGGCCACC. Plasmid pHIS-TEV-DYNLL2, which was used for the expression in *Escherichia coli* of DYNLL2 with an N-terminal six-histidine tag (His tag) spaced from DYNLL2 by a tobacco etch virus (TEV) protease cleavage site, was created by ligating *Nde*I- and *Eco*RI-digested pHIS-parallel 1 (*38*) with an *Eco*RV- and *Eco*RI-digested PCR fragment containing the mouse *Dynll2* ORF (amplified from plasmid DLC8B-pCMVsport using primers GATTACGATATCCCAACGACCGAAAACCTGTATTTTCAGGGCATGTCTGACCGGAAGGCAGTGATC and ATCGTAGAATTCACACCTTCGCCTCGGCCACCTAG) and with an *Nde*I- and *Eco*RV-digested DNA linker created by annealing two complementary oligonucleotides (forward oligonucleotide, GATATACATATGGCACATCACCATCACCATCACGATTACGATATCCCAACG). The following plasmids, which were used for the expression of myosin Va fragments fused to GST, were generated by ligating *Nco*I- and *Spe*I-digested PCR fragments of mouse brain myosin Va with *Nco*I- and *Spe*I-digested pGST-parallel 1 (*38*) (numbers indicate the residues of brain myosin Va; primers used for PCR amplification are denoted in parentheses): pGST-MVa-911−1194 (TAGCATCCATGGAGGCTCGCTCTGTGGAACGCTACAAGAAG and TAGCATACTAGTCATGGCCTTTCTTCTTCCTTTGCCTTGCTGC), pGST-MVa-1194−1316 (TAGCATCCATGGCGCCACAGATAAGAGGAGCTGAACTAG and TAGCATACTAGTCATTTCAAACCAATATATGCTTGTGCTATTTCACC), and pGST-MVa-1311−1422 (TAGCATCCATGGCATATATTGGTTTGAAAGAAACAAACAG and TAGCATACTAGTCACTCCATCTGCCCCACTTCTAGTTCACC). pGST-MVa-1194−1316-B was constructed as pGST-MVa-1194−1316, except that the br myosin Va cDNA lacking exon B was used as the template. pGST-MVa-1282−1291 was created by ligating an *Nco*I- and *Spe*I-digested pGST-parallel 1 with an *Nco*I- and *Spe*I-digested linker that was generated by annealing two complementary oligonucleotides (forward oligonucleotide, TAGCATCCATGGCTCCCAAGGATGACAAGAATACAATGACAGATTGACTAGTATGCTA). GST-GTD was cloned as described previously (*39*). PCR-amplified or mutagenized *Dynll* and myosin Va DNA fragments were verified by DNA sequencing.

Expression of Proteins in Sf9 Insect Cells and Copurification Experiments. Recombinant baculovirus stocks were produced by transfecting the baculovirus vectors into Sf9 cells as described previously (*9*). For protein expression, 100 mL cultures of Sf9 cells were co-infected for 3−4 days with viruses encoding calmodulin (*9*) and the indicated myosin Va heavy chain and DYNLL proteins. FLAG-tagged myosin Va was isolated from cell extracts using anti-FLAG M2 affinity gel (Sigma) as described previously (*9*). Cleared cell extracts, as well as the proteins eluted from the M2 beads using the FLAG peptide, were analyzed by SDS−PAGE, Western blotting, and immunodetection with anti-FLAG (Sigma M2), anti-HA (Zymed catalog number 32-6700), and anti-c-Myc (Zymed catalog number 13-2500) antibodies.

Purification of DYNLL2 and Myosin Va Fragments from E. coli. To produce DYNLL2 protein, BL21 Star (DE3) *E. coli* cells (Invitrogen) were transformed with pHIS-TEV-DYNLL2, grown to mid-logarithmic phase at 37 °C, and incubated for 8 h at 30 °C following addition of isopropyl β-D-thiogalactopyranoside (IPTG, final concentration of 1 mM) to induce expression. All protein purifications were carried out at 4 °C. For DYNLL2, cells from a 1 L culture

were resuspended in 16−20 mL of 50 mM Tris-HCl, 500 mM NaCl, 5 mM imidazole, and 5 mM β-mercaptoethanol (pH 8.0) containing 10 μg/mL leupeptin, 2 μg/mL pepstatin A, and 5 μg/mL aprotinin and lysed with a French press. The lysate was cleared by centrifugation (14500*g* for 30 min), and the supernatant was incubated on the rotating wheel for 2 h with 2.5 mL of Ni−NTA agarose (Qiagen). The Ni−NTA agarose was then washed with buffer A [50 mM Tris-HCl, 500 mM NaCl, and 20 mM imidazole (pH 8.0)] and the bound protein eluted with buffer B [50 mM Tris-HCl, 500 mM NaCl, and 350 mM imidazole (pH 8.0)]. When DYNLL2 was purified for the pull-down experiments used to estimate its affinity for myosin Va, buffers A and B were supplemented with 5 mM β-mercaptoethanol. After overnight dialysis against HIS-TEV buffer [50 mM Tris-HCl, 100 mM NaCl, and 1.0 mM DTT (pH 8.0)], the His tag was removed from DYNLL2 by incubation with 300−600 units of recombinant TEV protease. To separate DYNLL2 from the cleaved His tag and the TEV protease, the digested protein was incubated with Ni−NTA resin, yielding in the flow-through the untagged DYNLL2 modified only with an additional glycine, N-terminal to the first DYNLL2 residue (Met). DYNLL2 was either used directly in the in vitro pull-down assay shown in Figure 2 or dialyzed as described below for all other experiments.

To produce GST and various fragments of myosin Va fused to GST, BL21 Star (DE3) *E. coli* cells were transformed with pGST-parallel 1 or with pGST-parallel 1 harboring a myosin Va insert, grown to mid-logarithmic phase at 37 °C, and incubated for 2−4 h at 30 °C following addition of 1 mM IPTG. Cells from 130 mL cultures were resuspended in 10 mL of PBS containing a tablet of protease inhibitors (Complete Mini, Roche catalog number 11836153001) and lysed as described above. The lysate was cleared by centrifugation (12 000*g* for 10 min) and the supernatant incubated on a rotating wheel for 2 h with 0.45 mL of glutathione−Sepharose 4B beads (Amersham). Subsequently, the beads were washed with PBS and used directly in the in vitro pull-down assay shown in Figure 2. For the pull-down experiments designed to estimate the affinity of DYNLL2 for myosin Va (Figure 4A), the GST-tagged myosin Va fragments corresponding to brain myosin Va residues 1194−1316 (GST-MyoVa$^{1194-1316}$) and residues 1194−1316 lacking the three residues of exon B (GST-MyoVa$^{1194-1316}\Delta$ExonB) were purified as described above except that the PBS contained 1 mM DTT, and the GST fusion proteins were eluted with 100 mM NaCl, 200 mM Tris-HCl (pH 8.0), 1 mM DTT, and 20 mM glutathione.

To obtain MyoVa$^{1194-1316}$ and MyoVa$^{1194-1316}\Delta$ExonB for analytical ultracentrifugation, circular dichroism (CD) measurements, and cross-linking experiments, the glutathione−Sepharose beads charged with these proteins were incubated overnight with 100 units of TEV protease in 0.8 mL of HIS-TEV buffer. Myosin fragments modified by four additional residues (GAMA) at their N-terminus were recovered in the flow-through. After the flow-through was adjusted to 300 mM NaCl and 5 mM imidazole, the TEV protease was removed by incubation with 45 μL of Ni−NTA resin, which yielded TEV-free myosin Va fragments.

For ultracentrifugation, CD, and cross-linking experiments, purified MyoVa$^{1194-1316}$, MyoVa$^{1194-1316}\Delta$ExonB, and DYNLL2 were dialyzed against CD buffer [10 mM sodium phosphate and 100 mM NaCl (pH 7.8)]. For the pull-down experiments used to estimate the affinity of DYNLL2 for myosin Va, GST-MyoVa$^{1194-1316}$, GST-MyoVa$^{1194-1316}\Delta$ExonB, and DYNLL2 were dialyzed against CD buffer containing 1 mM DTT. The purity of the DYNLL2 and myosin Va protein preparations was evaluated by SDS−PAGE and Coomassie Blue staining. For ultracentrifugation, CD, and cross-linking experiments, the dialysate was used for protein dilutions, and protein concentrations were determined by measuring the UV absorption spectra with a diode array Hewlett-Packard 8453 spectrophotometer equipped with a Peltier temperature control device for maintaining a constant temperature of the cell holder. Spectra were recorded at 20 °C using a 600 μL volume and a 1 cm path length quartz cell. Protein spectra were corrected for buffer absorbance. The absorbance at 340 nm was used to correct for light scattering at other wavelengths. Specific absorption coefficients at 280 nm (20 °C) of 0.281 and 1.34 cm^2/mg for MyoVa$^{1194-1316}$ (or MyoVa$^{1194-1316}\Delta$ExonB) and DYNLL2, respectively, were calculated.

In Vitro Pull-Down Assays for Mapping the DYNLL2 Binding Site in Myosin Va. GST and GST-myosin Va fusion proteins bound to glutathione−Sepharose beads were incubated for 2 h at 4 °C with 17.8 μg (Figure 2A, left panel) or 8.9 μg (Figure 2A, right panel) of DYNLL2 in 600 μL of PBS containing 0.3% NP-40. After an aliquot (Input) was removed from the binding reaction mixture, the beads were washed four times with PBS containing 0.3% NP-40, resuspended in SDS loading buffer, and boiled (Pull-Down). In Figure 2A, left panel, input fractions corresponding to 2% of the total binding reaction mixture and pull-down fractions corresponding to 15% of the total binding reaction mixture were subjected to SDS−PAGE and Coomassie Blue staining (Figure 2A, right panel, fractions of 4 and 30%, respectively). Pull-down fractions corresponding to 0.5% of the total binding reaction mixture were analyzed by SDS−PAGE, Western blotting, and immunodetection using an affinity-purified anti-DYNLL antibody (generous gift of S. M. King).

Cross-Linking Assay. For chemical cross-linking, purified MyoVa$^{1194-1316}$ at a concentration of 5 μM was incubated at 24 °C in CD buffer containing the zero-length cross-linker 5 mM 1-ethyl-3-[3-(dimethylamino)propyl]carbodiimide hydrochloride (EDC) and 10 mM *N*-hydroxysulfosuccinimide (S-NHS) for 0−120 min. Aliquots of the reaction mixture were removed at the indicated time points and analyzed by SDS−PAGE and Coomassie Blue staining.

Estimation of the Affinity of DYNLL2 for GST-MyoVa$^{1194-1316}$ with an in Vitro Pull-Down Assay. Solutions containing the purified myosin Va fusion proteins GST-MyoVa$^{1194-1316}$ or GST-MyoVa$^{1194-1316}\Delta$ExonB and DYNLL2 at equimolar concentrations of 0.5, 1.0, 2.0, and 5.0 μM in CD buffer containing 1 mM DTT were incubated for 3 h at 4 °C on the rotating wheel. Glutathione−Sepharose beads were then added; the sample was mixed for 1 h, and the beads were sedimented by low-speed centrifugation. Identical volumes of the binding reaction mixture, removed before starting the incubation (input), and the supernatant after the pull-down assay were separated by SDS−PAGE. The gels were stained with Coomassie Blue, and the intensities of the GST-MyoVa$^{1194-1316}$, GST-MyoVa$^{1194-1316}\Delta$ExonB, and DYNLL2 bands were quantified using an

Odyssey scanner. The percentage of DYNLL2 not bound to the myosin Va-coated beads was calculated by comparing the amounts of DYNLL2 in the input versus the supernatant.

Analytical Ultracentrifugation. Beckman Optima model XL-A and XL-I analytical ultracentrifuges equipped with absorption optics and four-place AN-Ti rotors were used for sedimentation equilibrium experiments at 20 and 4 °C. Cells with carbon-filled six-channel centerpieces (12 mm) and plane quartz windows were employed. Proteins were loaded into the right side of each channel: 0.090 mL at relative concentrations of $\sim^1/_3$ (inner), $^2/_3$ (middle), and 1.0 (outer) with an absorbance of ~0.33 in the outer channel; 0.105 mL of reference dialysate buffer was placed in each left channel. At the beginning of each run, scans at 280 or 230 nm were made in the continuous mode (0.003 cm steps) with three averages at 3000 rpm to establish solvent and protein meniscii, plateau absorbances, and bottom radial positions for each channel. After rotors were accelerated to a higher speed for sedimentation equilibrium (19 000 rpm for DYNLL2, 24 000 rpm for MyoVa$^{1194-1316}$, and 12 000 rpm for a 1:1 mixture of MyoVa$^{1194-1316}$ and DYNLL2) at 4.0 or 20.0 °C, auto scans at 2 h intervals were made in 0.001 cm steps (step mode) with seven averages for a total of ~42 h before ending centrifuge runs. Sedimentation equilibrium was attained within 24−32 h, as evidenced by no time-dependent changes in gradients. Identical samples of freshly prepared and dialyzed MyoVa$^{1194-1316}$ were loaded into two cells and run at the same time in the two ultracentrifuges at 20.0 and 4.0 °C. Freshly prepared and dialyzed DYNLL2 and a 1:1 mixture of MyoVa$^{1194-1316}$ and DYNLL2 were also run simultaneously in the two ultracentrifuges at 4 °C. The density of the CD buffer was determined to be 1.0053 g/mL using the Anton-Paar model DMA-58 densitometer at 4.00 ± 0.01 °C. Protein-specific volumes were calculated to be 0.720 and 0.715 mL/g for MyoVa$^{1194-1316}$ and DYNLL2, respectively, from the amino acid compositions derived from DNA sequences and the values of Zamyatnin (*40*). Global, weighted fits of sedimentation equilibrium data obtained at three concentrations of MyoVa$^{1194-1316}$ to a model of reversible monomer−dimer association (with fully competent species present) were made using software provided by A. P. Minton (National Institute of Diabetes and Digestive and Kidney Diseases, National Institutes of Health). Baselines were held constant at zero absorbance at 280 or 230 nm (as predetermined by buffer−buffer runs). Trimers and tetramers were not detectable. For the 1:1 mixture of MyoVa$^{1194-1316}$ and DYNLL2, a heterologous association constant was determined using the program of J. L. Cole (University of Connecticut, Storrs, CT), which can be downloaded from the RASMB web site. For all accepted data, residuals from observed data and fits of data as a function of radial distance from the center of rotation to a monomer−dimer equilibrium (in the case of MyoVa$^{1194-1316}$) or to a dimer−dimer association (in the case of the MyoVa dimer association with dimeric DYNLL2) were randomly distributed around zero (0.00 ± 0.01 absorbance). For conversion of absorbance values of apparent association constants (K_{obs}) to the true concentration-dependent association constants, $K_{1,2}'$ values (expressed per molar concentration of monomer) for MyoVa$^{1194-1316}$, it was assumed that the extinction coefficient at 230 nm of the monomer does not change upon dimerization. Thus, $K_{obs} = A_2/A^2 = (2/\epsilon)K_{1,2}'$, where A is the specific absorbance of the monomer and the molar extinction coefficient (ϵ) is for a 1.2 cm path length. A monomer M_r value of 14 285 for MyoVa$^{1194-1316}$ was used to calculate ϵ, resulting in the equation $\log K_{1,2}' = 4.400 + \log K_{obs}$. For the association of dimeric MyoVa$^{1194-1316}$ with the DYNLL2 dimer, the molar extinction coefficient of each dimer at 230 nm with a 1.2 cm path length was estimated to be 100 500 $cm^2\ M^{-1}$.

Circular Dichroism. Far-UV circular dichroism (CD) measurements were performed with a Jasco-710 spectropolarimeter using a water-jacketed (1 mm path length) cylindrical quartz cell. The temperature of the cell was controlled by an external programmable water bath (Neslab RT-110). Proteins [MyoVa$^{1194-1316}$, MyoVa$^{1194-1316}$ΔExonB, DYNLL2, and 1:1 (mole) mixtures of MyoVa$^{1194-1316}$ and DYNLL2 and of MyoVa$^{1194-1316}$ΔExonB and DYNLL2] were assessed at protein monomer concentrations of 5 μM with mixtures containing each of the component proteins in CD buffer at 5 μM. CD spectra were recorded from 260 to 195 nm at 0.5 nm resolution and a scanning speed of 10 nm/min at 5, 20, and 25 °C. Each spectrum was an average of four accumulated spectra and was corrected for the solvent CD signal. The data were expressed as mean residue molar ellipticity units (degrees square centimeters per decimole) where the mean residue molecular weights of the proteins were 112.3 for MyoVa$^{1194-1316}$, 112.2 for MyoVa$^{1194-1316}$ΔExonB, and 115.4 for DYNLL2. In the cases of the MyoVa$^{1194-1316}$/DYNLL2 and MyoVa$^{1194-1316}$ΔExonB/DYNLL2 mixtures, the observed CD spectrum of DYNLL2 was subtracted from each observed spectrum and the resulting data were transformed to mean residue ellipticity values using the corresponding mean residue molecular weights for MyoVa$^{1194-1316}$ and MyoVa$^{1194-1316}$ΔExonB, respectively. We note that the subtracted spectra contain the noise from both measured spectra, that we did not smooth the spectra, and that similar results were obtained in two independent experiments. The helical content was estimated as described previously (*36*, *41*). The thermal unfolding of the proteins was studied by increasing the temperature of the samples (after measuring CD spectra) from 10 to 65 °C at a rate of 60 °C/h while recording the ellipticity value at 222 nm at 30 s intervals with a time constant of 16 s. Progress ellipticity curves for MyoVa$^{1194-1316}$ or MyoVa$^{1194-1316}$ΔExonB were analyzed by a two-state dissociation model as described previously (*42*).

Structure Prediction. Coiled-coil propensities were obtained with Coils (*43*) using a window width of 28, the MTIDK matrix, and weighting of heptad positions a and d by 2.5. Paircoil and Paircoil2 (*44*, *45*) gave similar results (not shown). Secondary structure prediction was performed using PSIPRED (*46*) and PredictProtein (*47*).

RESULTS

Exon B, an Alternatively Spliced Exon in the Myosin Va Heavy Chain, Is Required for DYNLL2−Myosin Va Interaction. To examine the interaction of DYNLL with myosin Va, we expressed a full-length, FLAG-tagged version of the brain-spliced heavy chain isoform of mouse myosin Va (see Figure 1A for a schematic of splice isoforms) together with calmodulin and DYNLL in insect cells and analyzed the ability of DYNLL to copurify with the myosin from cell

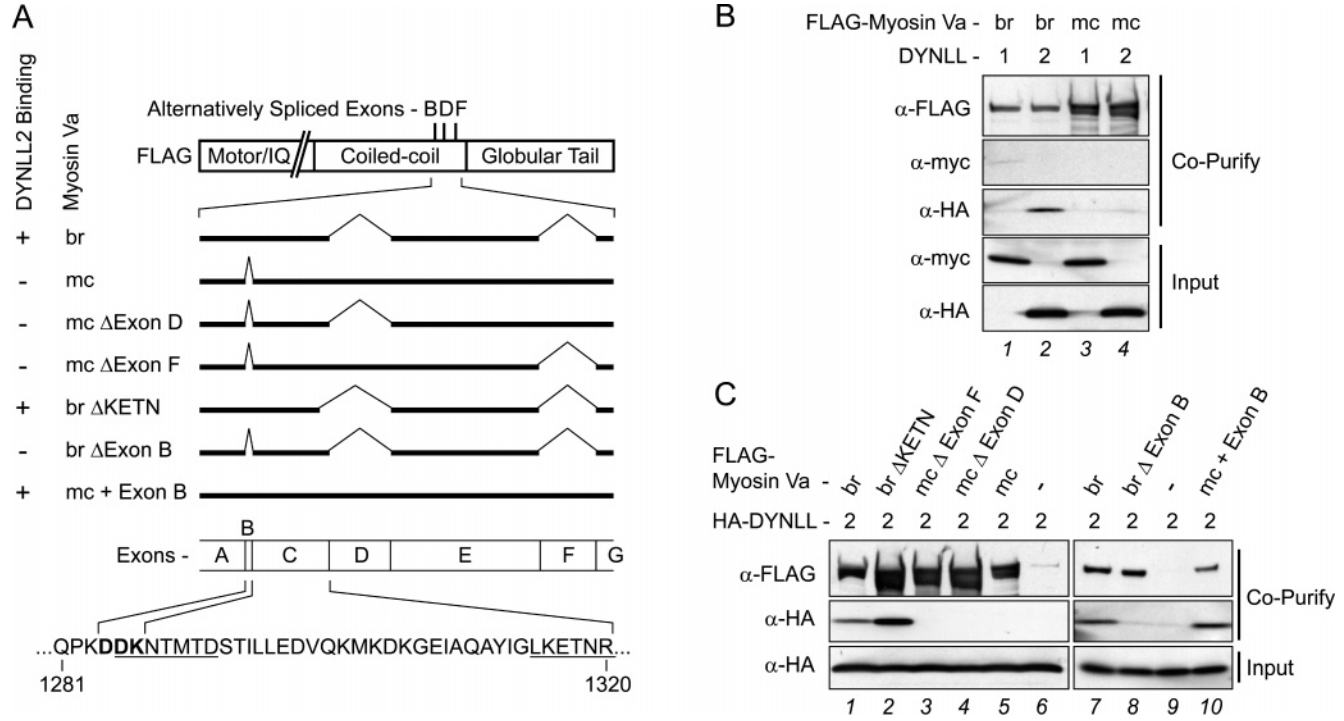

FIGURE 1: Mapping of the binding site for DYNLL2 within the heavy chain of mouse myosin Va. (A) The top part shows a schematic representation of the domain organization of the mouse myosin Va heavy chain. The heavy chain is drawn as an empty bar with the motor domain, IQ motifs, coiled-coil domain, globular tail domain, and approximate positions of the three alternatively spliced exons (B, D, and F) indicated. All full-length heavy chain constructs were tagged with the FLAG epitope tag at their N-termini. The middle part shows the region of alternative splicing within the heavy chain, which falls entirely within its central stalk domain, and which spans exons A−G, magnified and depicted by black horizontal bars (br, brain-spliced isoform; mc, melanocyte-spliced isoform). The various alternatively spliced versions of the myosin Va heavy chain used in this study are shown, and their ability to be copurified with DYNLL2 is summarized at the left. The bottom part shows the amino acid sequence of the portion of the brain-spliced heavy chain isoform of myosin Va that contains motifs that are similar to known DYNLL-binding sites (underlined). Exon B is in bold. (B) DYNLL2 copurifies with the brain-spliced heavy chain isoform but not with the melanocyte-spliced heavy chain isoform. Full-length, FLAG-tagged brain (br) or melanocyte (mc) heavy chain isoforms were coexpressed in Sf9 cells with calmodulin and either myc-tagged DYNLL1 or HA-tagged DYNLL2 as indicated. Myosin Va was purified from cell extracts using beads coated with anti-FLAG antibodies and the eluted fraction analyzed by SDS−PAGE, Western blotting, and immunodetection using the indicated antibodies (Co-Purify). Similar analyses of the extracts before purification are also shown (Input). (C) Exon B is required for the binding of DYNLL2 to myosin Va. The indicated full-length, FLAG-tagged versions of the myosin Va heavy chain were coexpressed in Sf9 cells with calmodulin and HA-tagged DYNLL2. Extracts (Input) and bound fractions (Co-Purify) were analyzed as described for panel B.

extracts. We initially determined which of the two highly related mammalian DYNLL proteins bind to the myosin in this context. As shown in Figure 1B, HA-tagged mouse DYNLL2 (lane 2), but not myc-tagged mouse DYNLL1 (lane 1), copurifies efficiently with the brain-spliced myosin isoform. These results are consistent with previous studies (*8*, *17*, *18*) showing that myosin Va purified from brain contains DYNLL and that the myosin preferentially binds DYNLL2.

In contrast to these results using the brain-spliced isoform, which contains exons A−C and E within the region of alternative splicing (Figure 1A), neither DYNLL isoform copurified with the melanocyte-spliced isoform (Figure 1B, lanes 3 and 4), which contains exons A and C−F within the same region (Figure 1A). These results suggest that exons B, D, and/or F, which distinguish the brain- and melanocyte-spliced isoforms from each other, dictate in some way the ability of myosin Va to bind DYNLL2. To address this issue, we performed copurification experiments with insect cells expressing different splice or mutant variants of the myosin Va heavy chain (Figure 1A,C). Theoretically, exon D (27 residues) or exon F (25 residues), each of which is present in the melanocyte-spliced isoform but not the brain-spliced isoform (Figure 1A), could act as a negative regulator of DYNLL2 binding. However, the omission of either exon D or exon F from the melanocyte-spliced isoform is not sufficient to induce its copurification with HA-DYNLL2 [Figure 1C; compare mc ΔExon D (lane 4) and mc ΔExon F (lane 3) to mc (lane 5) and br (lane 1)]. Moreover, the deletion from the brain-spliced isoform of four residues (KETN, residues 1316−1319), which fall at the exon D integration site (Figure 1A) and that contribute to what could be a consensus DYNLL binding site that would be disrupted by the insertion of exon D (**LKETNR**[exon D]**L**, where the bold residues denote the putative consensus site), does not abolish the ability of DYNLL2 to copurify with the myosin [Figure 1C; compare br ΔKETN (lane2) to br (lane1)].

Given these results, our attention turned to exon B as a possible positive regulator of DYNLL2 binding. As stated previously, this three-residue exon (DDK; residues 1284−1286) is specific to the brain-spliced isoform, where it falls within an ∼25 residue discontinuity in the central stalk domain that divides the second and third major sections of the predicted coiled coil (i.e., between CC2 and CC3; Figure 2B). Moreover, exon B constitutes part of a motif (*DDK*NT-MTD, residues 1284−1291; see Figure 1A) that resembles other DYNLL-binding sites and that is homologous to the peptide from chicken myosin Va that binds DYNLL1 in vitro

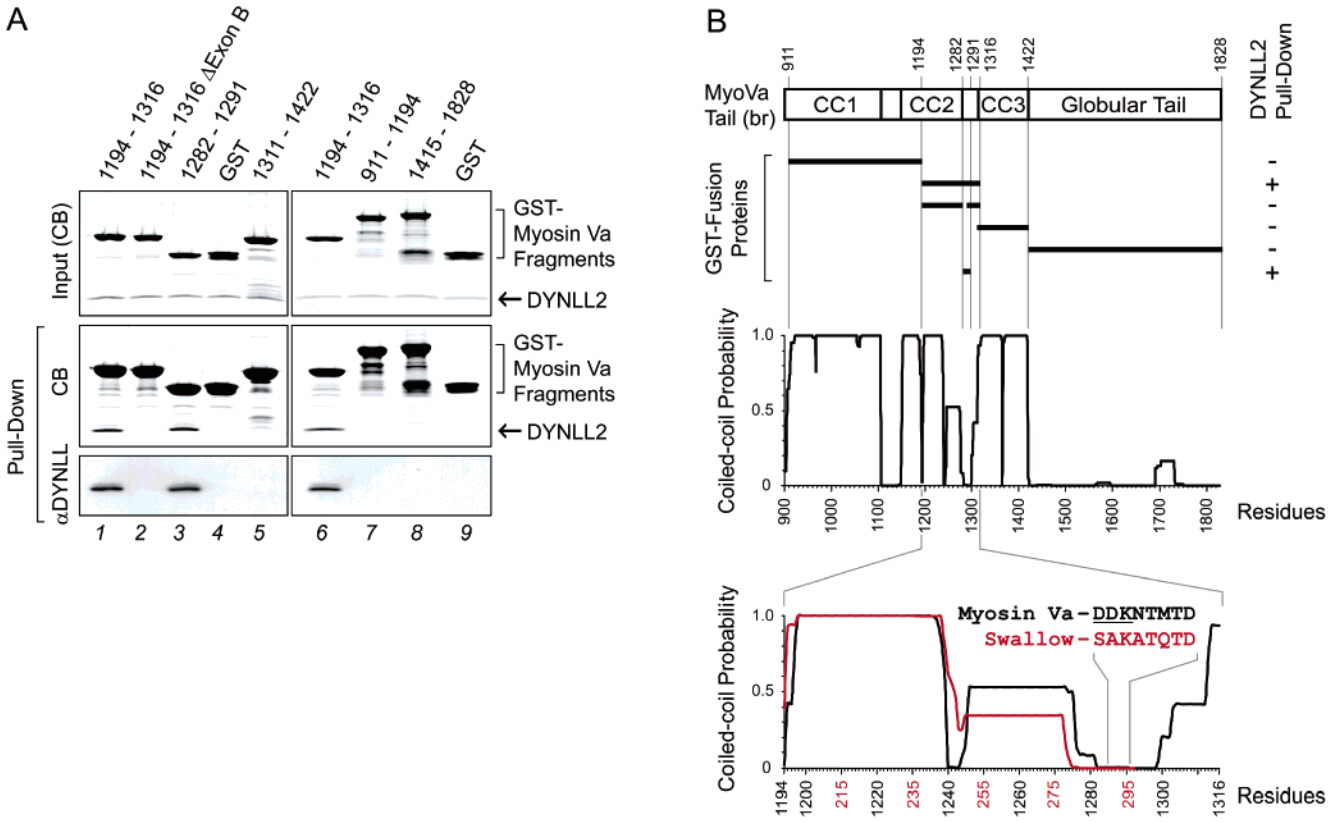

FIGURE 2: Identification of the DYNLL2-binding site in the myosin Va heavy chain. (A) In vitro pull-down assays. Various fragments of the tail domain of the brain-spliced heavy chain isoform (residue numbers at the top) were expressed as GST fusion proteins and, along with GST alone as a control, incubated with pure DYNLL2. The binding reaction mixture (Input) and the bound fraction obtained by pull-down using glutathione−Sepharose beads (Pull-Down) were analyzed by SDS−PAGE and Coomassie Blue staining (CB). DYNLL2 was also detected in pull-down samples by Western blotting using the anti-DYNLL antibody (αDYNLL). (B) Schematic representation of the tail domain of the brain-spliced heavy chain isoform of myosin Va (residue numbers are indicated; CC1, CC2, and CC3 indicate the three major sections of predicted coiled coil in the central stalk domain). The GST fusion proteins used in the pull-down experiments in panel A are depicted below, and their ability to bind DYNLL2 is summarized at the right. The middle graph shows the probability of forming an α-helical coiled coil for the tail domain of mouse brain myosin Va (residues 900−1828), while the bottom graph shows the probability of forming a coiled coil for MyoVa$^{1194-1316}$, the fragment of the brain isoform used in Figures 3−6 (residues 1194−1316, black line). For comparison, the bottom graph also shows the probability of forming a coiled coil for the fragment of the swallow protein used by Wang et al. (*36*) (GenBank entry NP_511060, residues 199−297, red line). The respective amino acid residues are indicated (myosin Va, black numbers; swallow, red numbers). The binding of DYNLL is known to promote the dimerization and coiled-coil assembly of this swallow fragment (*36*). Coiled-coil predictions were performed using Coils as described in Materials and Methods. A score of 1.0 indicates 100% probability of forming a coiled coil. The coiled-coil predictions for the fragment of myosin Va used here and the fragment of swallow used in ref *36* are aligned in the bottom graph so that their DYNLL-binding sites are at the same position. These binding site sequences are written in black for myosin Va (residues 1284−1291, exon B underlined) and red for swallow (residues 289−296).

(*33*). Figure 1C shows that the deletion of exon B from the brain-spliced isoform completely abrogates its interaction with HA-DYNLL2 [Figure 1C; compare br ΔExon B (lane 8) to br (lane 7)]. Even more strikingly, the insertion of exon B into the melanocyte-spliced isoform is sufficient to confer on it the ability to copurify with DYNLL2 [Figure 1C; compare mc + Exon B (lane 10) to br (lane 7)]. We conclude, therefore, that exons D and F do not block DYNLL2 binding and that exon B is required for DYNLL2 binding.

Exon B and Seven Adjacent Residues Are Sufficient To Bind DYNLL2. The results given above suggest that the DYNLL-binding consensus motif that contains exon B (residues 1285−1291) is an essential part of a DYNLL-binding site in the myosin Va heavy chain. To verify this, we performed pull-down assays using GST fusion proteins containing portions of the tail domain of the brain-spliced isoform (see Figure 2B) together with recombinant, His-tagged DYNLL2 (from which we first removed the His tag). Figure 2A shows that while purified DYNLL2 binds to a GST fusion protein containing the central portion of the coiled-coil stalk domain that includes exon B (residues 1194−1316, lanes 1 and 6), it does not bind to GST alone (lanes 4 and 9) or to GST fusion proteins containing the first portion of the coiled-coil stalk domain (residues 911−1194, lane 7), the last portion of the coiled-coil stalk domain (residues 1311−1422, lane 5), or the globular tail domain (residues 1415−1828, lane 8). Moreover, the deletion of exon B from the GST fusion protein containing residues 1194−1316 abolishes its ability to bind DYNLL2 (Figure 2A; compare lane 2 to lane 1). Finally, we found that a GST fusion protein containing just residues 1282−1291 (PKD-DKNTMTD), which include exon B (DDK) and five following residues that together resemble the DYNLL binding site in other proteins (*27*, *33*), is sufficient to bind DYNLL2 (Figure 2A, lane 3). We conclude, therefore, that the myosin V heavy chain contains a single DYNLL binding site, that this site resides in a relatively short stretch of sequence that falls within a discontinuity in the central coiled-coil stalk domain, that it resembles other DYNLL binding

sites, and that it requires the presence of exon B.

A Fragment of Myosin Va Containing Residues 1194−1316 Is a Dimer at 4 °C and Binds DYNLL2 with an Affinity of ~3 × 10⁶ M⁻¹. As in the swallow protein, the DYNLL2-binding site in myosin Va resides in a region that is not predicted to form an α-helical coiled coil but that is located immediately C-terminal of regions predicted to form a coiled coil, albeit with variable probability (Figure 2B). As described in the introductory section, the binding of DYNLL to the swallow protein promotes the formation of an α-helical coiled-coil structure in a region of swallow immediately N-terminal of its DYNLL binding site (*36*). Similarly, the dynein intermediate chain IC74 gains α-helicity and possibly α-helical coiled-coil structure upon binding DYNLL (*35*). Together, these observations prompted us to investigate whether the binding of DYNLL to myosin Va alters the supersecondary structure of its heavy chain in regions immediately adjacent to its DYNLL binding site. To test this possibility, we used purified DYNLL2 and a purified fragment of the brain myosin Va heavy chain containing residues 1194−1316. This portion of myosin Va, shown in detail in the bottom part of Figure 2B and hereafter designated MyoVa$^{1194-1316}$, contains from the N- to C-terminus 38 residues with 100% probability of forming an α-helical coiled coil (approximately five heptads), a stretch of 11 residues containing three helix-breaking proline residues, 30 residues with ~50% probability of forming an α-helical coiled coil (approximately four heptads), a stretch of nine residues containing a proline, the DYNLL binding site (underlined), and 23 C-terminal residues with an increasing probability of forming a coiled coil. Figure 2B also shows (red) that the region of swallow containing its DYNLL binding site is very similar to MyoVa$^{1194-1316}$ with regard to predicted α-helical coiled-coil content. The region of swallow between residues 206 and 275 is thought to assume a stable α-helical coiled-coil structure upon DYNLL binding (*36*).

We first characterized the self-association status of the MyoVa$^{1194-1316}$ fragment. Unless stated otherwise below, the protein was used following cleavage of the GST moiety and purification of the myosin fragment. Preliminary evidence that MyoVa$^{1194-1316}$ readily forms a dimer came from cross-linking experiments using the zero-length cross-linker EDC/S-NHS, where the monomeric fragment was seen to convert rapidly into a protein species with twice the mass (Figure 3). More importantly, sedimentation equilibrium centrifugation of MyoVa$^{1194-1316}$ showed that this fragment exhibits a temperature-dependent monomer−dimer equilibrium with self-association constants of ~2 × 10⁶ (M subunit)$^{-1}$ at 20 °C (i.e., a K_D of ~0.6 μM) and ~3 × 10⁷ (M subunit)$^{-1}$ at 4 °C (i.e., a K_D of ~0.03 μM; Table 1). Global analysis of the data obtained from sedimentation equilibrium centrifugation of DYNLL2 at 4 °C also indicated that DYNLL2 is a dimer with an M_r of 20 800 at concentrations of 1−3 μM (Table 1).

To estimate the affinity of DYNLL2 for MyoVa$^{1194-1316}$, we performed both pull-down assays and sedimentation equilibrium centrifugation. For the pull-down assays, equimolar mixtures of MyoVa$^{1194-1316}$ (used here as an uncleaved GST fusion protein) and DYNLL2 (5, 2, 1, and 0.5 μM) were incubated at 4 °C for 3 h. The mixtures were then incubated with an excess of glutathione−Sepharose beads,

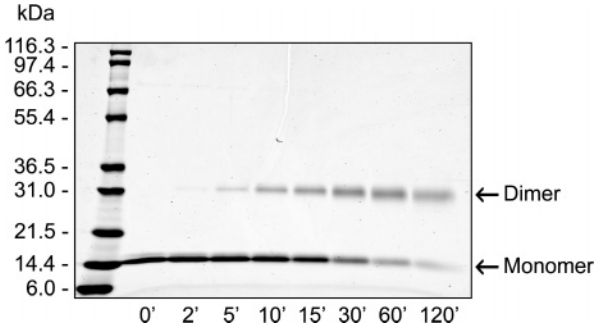

FIGURE 3: Detection of MyoVa$^{1194-1316}$ dimerization by chemical cross-linking. MyoVa$^{1194-1316}$ (5 μM) was incubated at 24 °C with 5 mM EDC and 10 mM S-NHS in 10 mM sodium phosphate and 100 mM NaCl (pH 7.8) for the time (minutes) indicated. The samples were then analyzed by SDS−PAGE and Coomassie Blue staining. The molecular weights of the standard proteins loaded in the first lane are given at the left. Protein species corresponding in molecular weight to monomeric (Monomer) and dimeric (Dimer) forms of MyoVa$^{1194-1316}$ were detected. We note that species larger than the dimer were not detected, suggesting that cross-linking is detecting a physiological species.

and GST-MyoVa$^{1194-1316}$ together with any associated DYNLL2 was pelleted by low-speed centrifugation of the resin. To calculate the percentage of DYNLL2 bound, the amount of DYNLL2 remaining in the supernatant was determined by quantitative laser densitometry following SDS−PAGE [Figure 4A (●)]. The finding that only ~30% of the total DYNLL2 in the binding reaction mixture remained in the supernatant when both proteins were used at a concentration of 0.5 μM suggests that the dissociation constant (K_D) for the interaction between DYNLL2 and MyoVa$^{1194-1316}$ is tighter than 0.5 μM. As expected, omission of exon B from GST-MyoVa$^{1194-1316}$ greatly reduced its affinity for DYNLL2; at 0.5 μM for both proteins, ~90% of the total DYNLL2 in the reaction mixture remained in the supernatant using GST-MyoVa$^{1194-1316}$ΔExonB [Figure 4A (○)]. Consistent with these results, sedimentation equilibrium centrifugation of mixtures containing equimolar concentrations of both MyoVa$^{1194-1316}$ and DYNLL2 at 4 °C yielded a heterologous association constant of ~3 × 10⁶ M^{-1} for formation of the complex between MyoVa$^{1194-1316}$ dimers and DYNLL2 dimers (i.e., a K_D of ~0.4 μM; Table 1). Figure 4B shows a representative global fit of the data to a model for the heterologous association of dimeric MyoVa$^{1194-1316}$ and DYNLL2 to form the complex [$(MyoVa)_2$−$(DYNLL2)_2$]. The residuals of the fit (Figure 4B, top panel) are well within ±0.01 absorbance unit at 230 nm. Together, these data argue that DYNLL2 binds MyoVa$^{1194-1316}$ with a submicromolar affinity.

Circular Dichroism Spectroscopy Reveals a Structural Change in MyoVa$^{1194-1316}$ upon DYNLL2 Binding. We used far-UV circular dichroism (CD) measurements to investigate the possibility that the binding of DYNLL2 to MyoVa$^{1194-1316}$ alters its structure. We first determined the CD spectrum of MyoVa$^{1194-1316}$ alone at 5 °C and at a concentration of 5 μM, conditions where sedimentation equilibrium centrifugation shows that MyoVa$^{1194-1316}$ is essentially entirely dimeric. The resulting spectrum shows double minima at 208 and 222 nm, consistent with the presence of α-helical structure (Figure 5, black line). We note that the value of the ratio $[\theta_{222}]/[\theta_{208}]$ for MyoVa$^{1194-1316}$ is 0.86. Regions of proteins that are α-helical but not coiled coil typically have a $[\theta_{222}]$/

Table 1: Sedimentation Equilibrium Results[a]

sample	species present	T (°C)	λ (nm)	association constant, K_A' (M^{-1})
DYNLL2[b]	dimer	4	280	10^8 [5]
MyoVa$^{1194-1316}$ [c]	monomer/dimer	20	230	$(1.7 \pm 0.1) \times 10^6$ [8]
MyoVa$^{1194-1316}$ [c]	monomer/dimer	4	230	$(3.1 \pm 0.5) \times 10^7$ [4]
1:1 mixture of MyoVa$^{1194-1316}$ and DYNLL2[d]	dimer + dimer/tetramer	4	230	$(2.6 \pm 0.4) \times 10^6$ [5]

[a] Global analyses of sedimentation equilibrium data obtained at either 280 or 230 nm after equilibrium were obtained for proteins in 10 mM sodium phosphate and 100 mM NaCl (pH 7.8) using six-channel centerpieces for three concentrations of protein (see Materials and Methods). The numbers in brackets after the K_A' values are the number of global fits of data analyzed at 2 h intervals; the mean values of K_A' with standard mean deviations are given. [b] For DYNLL2 (M_r = 10 400 subunit), only the dimer was detected; 10^8 for K_A' is the limit of the method. [c] For MyoVa (M_r = 14 285 subunit), global analyses showed a monomer−dimer equilibrium with K_A' values (expressed per molar subunit) given for both 4 and 20 °C. [d] For the 1:1 equimolar mixture of dimeric MyoVa (M_r = 28 600) and dimeric DYNLL2 (M_r = 20 800), the heterologous association constant was determined from global fits of data obtained after 34−40 h at 12 000 rpm (4 °C); see Figure 4B.

[θ_{208}] ratio of 0.83, whereas regions that are α-helical and also form coiled coils typically exhibit a [θ_{222}]/[θ_{208}] ratio of 1.03 (*35*, *36*, *48*−*50*).

To obtain the spectrum of MyoVa$^{1194-1316}$ in the presence of DYNLL2, the CD signal measured for 5 μM DYNLL2 alone (Figure 5, green line) was subtracted from the CD signal measured for the mixture of DYNLL2 and MyoVa$^{1194-1316}$ (each protein at 5 μM). In doing this, we are assuming, as have others (*35*, *36*), that the structures of free DYNLL and DYNLL bound to its target protein are the same. This assumption seems reasonable because DYNLL is a stably folded protein (*29*) and because NMR studies have shown that the secondary structure of DYNLL remains unchanged upon the binding of target peptides (*28*, *32*).

As shown in Figure 5 (red line), the ellipticity of MyoVa$^{1194-1316}$ around 222 nm becomes more negative in the presence of DYNLL2, indicating a slight increase in helical content (from 37% of MyoVa$^{1194-1316}$ residues in the α-helical conformation in the absence of DYNLL to 40% in the presence of DYNLL2; calculated as described in Materials and Methods). Moreover, the value of [θ_{222}]/[θ_{208}] for MyoVa$^{1194-1316}$ increases from 0.86 in the absence of DYNLL2 to 1.01 in the presence of DYNLL2. This change is consistent with the introduction of coiled-coil structure into the MyoVa$^{1194-1316}$ fragment upon DYNLL2 binding or with an increase in its content of coiled coil upon DYNLL binding (see Discussion for details).

To determine if the observed effects of DYNLL2 on the structure of MyoVa$^{1194-1316}$ depend on the ability of DYNLL2 to bind MyoVa$^{1194-1316}$, we determined the CD spectrum of MyoVa$^{1194-1316}$ΔExonB in the presence and absence of DYNLL2 (Figure 5, dashed red and black lines, respectively). As demonstrated above, DYNLL2 has little if any ability to bind to a MyoVa$^{1194-1316}$ when the three amino acids corresponding to exon B have been deleted. Consistent with this, the spectrum of MyoVa$^{1194-1316}$ΔExonB remains essentially unchanged after the addition of DYNLL2. Specifically, the [θ_{222}]/[θ_{208}] values for MyoVa$^{1194-1316}$ΔExonB are 0.86 and 0.89 in the absence and presence of DYNLL2, respectively, and the α-helical content is 37% in both cases. We conclude, therefore, that the observed effects of DYNLL2 on the structure of MyoVa$^{1194-1316}$ are specific and depend on the ability of DYNLL2 to bind to this segment of the myosin Va coiled-coil domain.

The Binding of DYNLL2 Stabilizes MyoVa$^{1194-1316}$ against Thermal Unfolding. To obtain further evidence that the binding of DYNLL2 to MyoVa$^{1194-1316}$ alters the structure of MyoVa$^{1194-1316}$, we monitored changes in the CD signal of MyoVa$^{1194-1316}$ during thermally induced unfolding in the presence and absence of DYNLL2 (Figure 6). While no transition is observed for DYNLL2 alone (◇), the progress curve at 222 nm for MyoVa$^{1194-1316}$ alone (○) shows a loss of secondary structure as the temperature is increased [in Figure 6, the solid lines indicate the fits of the data to a two-state unfolding model with a linked dissociation of the dimer and the arrows indicate the transition midpoints or T_m values; Table 2 lists these T_m values, as well as the van't Hoff enthalpies (ΔH) for the fitted curves]. Strikingly, the T_m value for MyoVa$^{1194-1316}$ increases from 34.7 °C in the absence of DYNLL2 (○) to 42.1 °C in the presence of an equimolar amount of DYNLL2 (△). Because no significant thermal unfolding is observed for DYNLL2 alone at temperatures up to 65 °C, we conclude that this increase in T_m is due to the stabilization of MyoVa$^{1194-1316}$. Importantly, the T_m value for MyoVa$^{1194-1316}$ΔExonB alone (□), which has little if any ability to bind DYNLL2, does not increase upon addition of an equimolar amount of DYNLL2 (▽) (Figure 6). We conclude, therefore, that the binding of DYNLL2 to MyoVa$^{1194-1316}$ stabilizes the myosin fragment to thermal denaturation. These results are consistent with the idea that this interaction introduces (or increases the amount of) coiled-coil structure in MyoVa$^{1194-1316}$, since coiled coils are typically more stable to thermal denaturation than regions that are simply helical.

DISCUSSION

The functional significance of the variability generated in the myosin Va heavy chain protein sequence by the alternative splicing of exons B, D, and F is only partially understood. Previous work has shown that exon F is required for the interaction of the melanocyte-spliced isoform of myosin Va with melanophilin, an essential component of the melanosome receptor for myosin Va (*6*, *37*, *51*−*53*). Consistent with this, the ability of myosin Va to influence the distribution of melanosomes in living melanocytes is absolutely dependent on the presence of exon F (*6*, *37*, *54*−*57*). In the study presented here, we show that the heavy chain of the brain-spliced isoform of myosin Va possesses a single binding site for DYNLL2 and that this site resides within a discontinuity in the myosin's central coiled-coil stalk domain. Importantly, exon B constitutes an essential part of this DYNLL2 binding site. Omission of exon B from the brain-spliced isoform abrogates its interaction with DYNLL2, while introduction of this three-residue exon into the melanocyte-spliced isoform confers on it the ability to bind DYNLL2. In vivo, therefore, the spliced isoform expressed

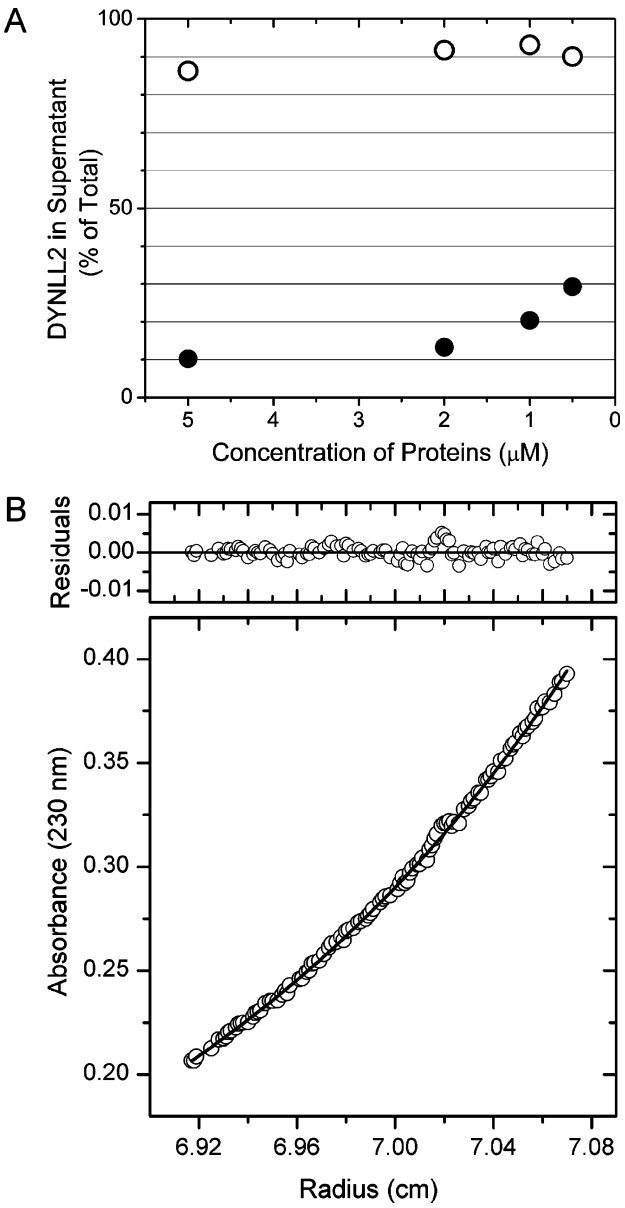

FIGURE 4: Determination of the affinity of DYNLL2 for MyoVa$^{1194-1316}$. (A) GST pull-down assay. Equimolar mixtures of DYNLL2 and GST-MyoVa$^{1194-1316}$ or GST-MyoVa$^{1194-1316}$ΔExonB were incubated for 3 h in 10 mM sodium phosphate and 100 mM NaCl (pH 7.8) at 4 °C before the GST-tagged protein and bound DYNLL2 were collected using glutathione−Sepharose beads (see Materials and Methods). The graph shows the percentage of total DYNLL2 added to the assay that remained in the supernatant after bead pull-down for equimolar mixtures containing DYNLL2 and GST-MyoVa$^{1194-1316}$ (●) or DYNLL2 and GST-MyoVa$^{1194-1316}$ΔExonB (○) at the indicated concentrations. (B) Sedimentation equilibrium of a 1:1 mixture of a MyoVa$^{1194-1316}$ dimer and a DYNLL2 dimer after 36 h at 12 000 rpm in 10 mM sodium phosphate and 100 mM NaCl (pH 7.8) at 4 °C, using a six-channel centerpiece (12 mm) with loading concentrations for inner, middle, and outer channels of ~0.6, 1.2, and 1.8 μM, respectively, for each dimeric protein. The data in the bottom panel are the absorbance at 230 nm (○) in the outer channel, and the solid line shows the global fit of the three concentrations to a heterologous association model for $(\text{MyoVa}^{1194-1316})_2 + (\text{DYNLL2})_2 \leftrightarrow (\text{MyoVa}^{1194-1316})_2-(\text{DYNLL2})_2$ with a K_A' of $(3.9 \pm 1.4) \times 10^6$ M^{-1}. Residuals are shown in the top panel.

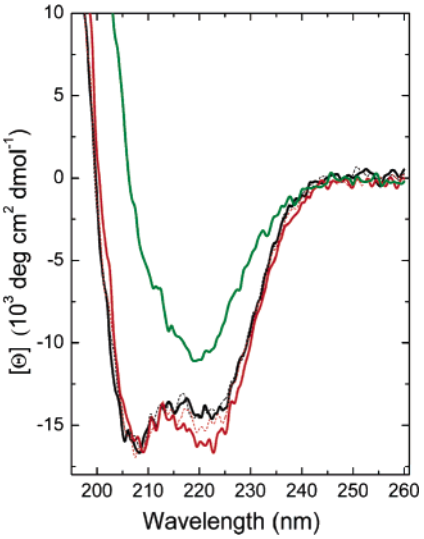

FIGURE 5: Binding of DYNLL2 causes a change in the far-UV CD spectrum of MyoVa$^{1194-1316}$. Shown are the far-UV CD spectra at 5 °C for 5 μM MyoVa$^{1194-1316}$ alone (black line), 5 μM MyoVa$^{1194-1316}$ΔExonB alone (dashed black line), 5 μM DYNLL2 alone (green line), 5 μM MyoVa$^{1194-1316}$ and 5 μM DYNLL2 (red line), and 5 μM MyoVa$^{1194-1316}$ΔExonB and 5 μM DYNLL2 (dashed red line) in 10 mM sodium phosphate and 100 mM NaCl (pH 7.8). The spectra for the latter two mixtures were calculated as described in Materials and Methods by subtracting the spectrum obtained for 5 μM DYNLL2 alone from the spectra of the mixtures of DYNLL and either MyoVa$^{1194-1316}$ or MyoVa$^{1194-1316}$ΔExonB. The change in the MyoVa$^{1194-1316}$ spectrum after the addition of DYNLL2 was observed in two independent experiments. The graph shows the unsmoothened spectra from a representative experiment.

in brain (exons ABCE), but not the spliced isoform that functions in melanosome transport (exons ACDEF), associates with DYNLL2. Together with previous work (*6*, *37*), our results show that alternative splicing controls the interaction of myosin Va with DYNLL2 (via exon B) as well as with melanophilin (via exon F). Given that DYNLL probably serves to link myosin Va with certain cargo molecules (*16*, *17*), the results presented here represent a second example of how the alternative splicing of myosin Va is used to specify its interaction with cargo. Phosphorylation of DYNLL and/or the DYNLL-binding site in myosin Va might also regulate DYNLL−myosin Va interaction, as it does for other DYNLL−target protein interactions (*58*, *59*).

We used DYNLL2 rather than DYNLL1 in our experiments with MyoVa$^{1194-1316}$ because only DYNLL2 copurified efficiently with full-length myosin Va in our assays. This result is consistent with sequence analyses of tissue-purified myosin Va, which indicated that DYNLL2 is the predominant DYNLL isoform bound to myosin Va in vivo (*8*, *17*). That said, we did see a very weak interaction of DYNLL1 with myosin Va, and we cannot rule out the possibility that in certain cellular contexts (e.g., high-level expression of DYNLL1 and no expression of DYNLL2) myosin Va may be associated with significant amounts of DYNLL1. Our findings do not agree, however, with previous observations made using yeast two-hybrid assays and in vitro pull-down experiments where both DYNLL isoforms appeared to interact equally well with myosin Va (*16*).

It has been suggested that DYNLL may serve to link myosin Va to other DYNLL-interacting proteins such as Bmf and GKAP, i.e., that DYNLL may serve as a cargo adaptor for myosin Va (*16*, *17*). This proposal is based on the fact that the DYNLL homodimer possesses two identical target

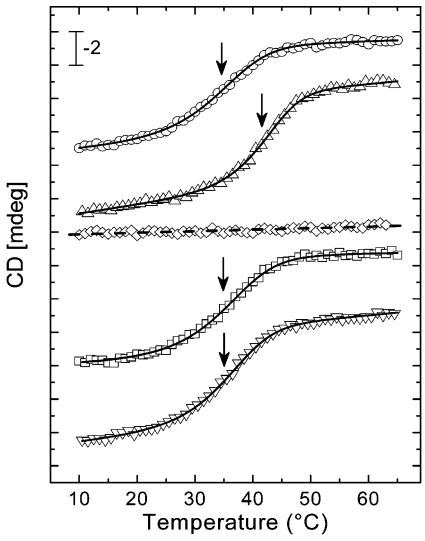

FIGURE 6: Binding of DYNLL2 stabilizes MyoVa$^{1194-1316}$ against thermal unfolding. Shown from top to bottom are the changes in ellipticity at 222 nm as a function of an increasing temperature (60 °C/h) for 5 μM MyoVa$^{1194-1316}$ alone (○), 5 μM MyoVa$^{1194-1316}$ and 5 μM DYNLL2 (△), 5 μM DYNLL2 alone (◇), 5 μM MyoVa$^{1194-1316}$ΔExonB alone (□), and 5 μM MyoVa$^{1194-1316}$ΔExonB and 5 μM DYNLL2 (▽). All assays were performed in 10 mM sodium phosphate and 100 mM NaCl (pH 7.8). Fits of the data to a two-state unfolding model coupled to dissociation of MyoVa$^{1194-1316}$ or MyoVa$^{1194-1316}$ΔExonB (see Materials and Methods) are shown as solid lines, while a linear regression fit to the data for DYNLL2 alone is shown as a dashed line. Each data set is shifted along the *Y*-axis with the units between the major tick marks equal to −2 mdeg. Plateau values at 65 °C are −1.7 mdeg for MyoVa$^{1194-1316}$ and MyoVa$^{1194-1316}$ΔExonB and −6.6 mdeg for DYNLL2. Determination of the CD spectrum before and after heating showed full reversibility of the unfolding in all cases. Arrows indicate the positions of the transition midpoint temperatures obtained from the fitting procedure (summarized in Table 2).

Table 2: Transition Midpoint Temperatures and van't Hoff Enthalpies of Unfolding for MyoVa$^{1194-1316}$, MyoVa$^{1194-1316}$ΔExonB, and 1:1 Mixtures of MyoVa$^{1194-1316}$ and DYNLL2 and of MyoVa$^{1194-1316}$ΔExonB and DYNLL2 (each component at 5 μM)[a]

protein	T_m (°C)	ΔH_{vH} (kcal/mol)
MyoVa$^{1194-1316}$	34.7	63
MyoVa$^{1194-1316}$ΔExonB	35.7	63
MyoVa$^{1194-1316}$ and DYNLL2	42.1	87
MyoVa$^{1194-1316}$ΔExonB and DYNLL2	35.8	69

[a] For each experiment, the transition midpoint temperature (T_m ± 0.3 °C) and van't Hoff enthalpy of unfolding (ΔH_{vH} ± 5%) were obtained by fitting the progress ellipticity data at 222 nm shown in Figure 6 to a two-state unfolding model coupled to dissociation (see Materials and Methods).

binding sites (*26*), thereby making it capable in principle of cross-linking two different proteins that contain a DYNLL binding site (*16*, *17*, *21*−*24*, *28*, *34*). To serve as a cargo adaptor, then, one face of the DYNLL dimer would bind to one of the two myosin Va heavy chains, while the other face would bind to the cargo molecule. While such an interaction is certainly possible, in the absence of negative cooperativity, the kinetically favored interaction of DYNLL bound to one of the two myosin Va heavy chains would most likely be to bind to the other heavy chain rather than to a cargo molecule. The resulting cross-link that would be generated between the two myosin Va heavy chains by this favored reaction could have important consequences for the conformation of the heavy chains in the vicinity of the DYNLL binding site. Consistent with this idea, we found that the binding of DYNLL2 to MyoVa$^{1194-1316}$, a fragment of the myosin's central stalk domain that contains its DYNLL2 binding site (^{1285}DKNTMTD) preceded by two putative coiled coils (one predicted with high probability, the other with low probability), results in the stabilization of MyoVa$^{1194-1316}$ against thermal denaturation and an increase in its α-helical coiled-coil content. We assume that these effects result from one DYNLL2 homodimer binding simultaneously to both heavy chain strands in MyoVa$^{1194-1316}$.

A previous study showed that the binding of DYNLL to a fragment of the swallow protein promotes the dimerization of the fragment and the formation of an α-helical coiled coil within it (*36*). The size, predicted content of the α-helical coiled coil, and domain organization of this swallow fragment are very similar to those of MyoVa$^{1194-1316}$ (i.e., a DYNLL binding site C-terminal of two short segments of predicted coiled coil, with only the more N-terminal one being strongly predicted to form a coiled coil; see Figure 2B, bottom). One apparent difference between that study and ours is that while the swallow fragment is only a weak dimer in the absence of DYNLL [$K_D \sim 4$ μM at 20 °C (*36*)], MyoVa$^{1194-1316}$ forms a tight dimer in the absence of DYNLL, especially at lower temperatures ($K_D \sim 0.6$ μM at 20 °C, and $K_D \sim 0.03$ μM at 4 °C). Importantly, the far-UV CD spectra of MyoVa$^{1194-1316}$ measured at 5 °C and at a concentration of 5 μM, conditions where it is essentially entirely dimeric before the addition of light chain, showed that its structure is changed significantly upon binding of DYNLL2. We believe, therefore, that this observed structural change is not a consequence of DYNLL2 promoting the dimerization of MyoVa$^{1194-1316}$ (see the model in Figure 7). Rather, we think that the binding of DYNLL2 alters the structure of MyoVa$^{1194-1316}$ even when it is already dimeric, as it certainly is in the context of native, full-length myosin Va.

In terms of the structural change induced in MyoVa$^{1194-1316}$ upon DYNLL binding, we found that the value of $[\theta_{222}]/[\theta_{208}]$ for MyoVa$^{1194-1316}$ increases from 0.86 in the absence of DYNLL2 to 1.01 in the presence of DYNLL2. Typical non-coiled-coil α-helical proteins show a $[\theta_{222}]/[\theta_{208}]$ value of 0.83, while this value is 1.03 for typical coiled-coil α-helices (*35*, *36*, *48*−*50*). If we adhere to these guidelines, then the change in the far-UV CD spectrum of MyoVa$^{1194-1316}$ upon DYNLL2 binding indicates the introduction of α-helical coiled-coil structure within it, i.e., that MyoVa$^{1194-1316}$ lacks coiled coil in the absence DYNLL2 and possesses coiled coil in the presence of DYNLL2. While certainly possible, the fact remains that MyoVa$^{1194-1316}$ is essentially entirely dimeric prior to the addition of DYNLL. Given this, and the fact that the only obvious way for MyoVa$^{1194-1316}$ to homodimerize on its own is via the formation of a coiled coil by its N-terminal 38 residues, which have a 100% probability of forming a coiled coil, we favor the idea that the increase in the value of $[\theta_{222}]/[\theta_{208}]$ upon DYNLL2 binding actually reflects an increase in the α-helical coiled-coil content of MyoVa$^{1194-1316}$ due to the DYNLL-dependent assumption of coiled-coil structure in the central, 30-residue segment of MyoVa$^{1194-1316}$ (residues 1246−1275, which exhibit a 50% probability of forming a coiled coil on their own). This scenario is presented schematically in the model

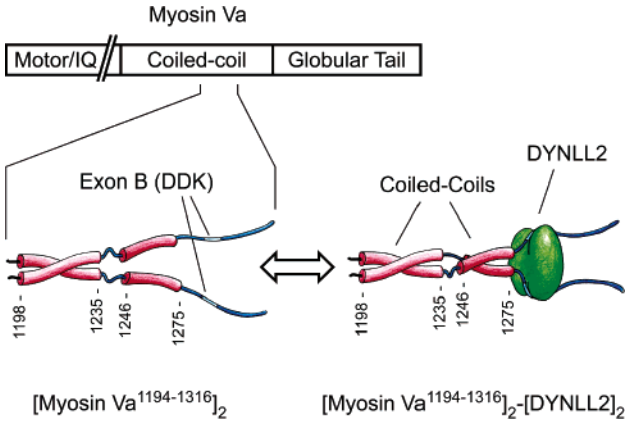

FIGURE 7: Hypothetical model for the structural change that occurs in MyoVa$^{1194-1316}$ upon binding of DYNLL2. MyoVa$^{1194-1316}$ is a fragment of myosin Va's central coiled-coil stalk domain and behaves as a dimeric target for DYNLL2, just as it must in the context of full-length myosin Va. The dimerization of this fragment is probably due to the formation of a short stretch of coiled coil by residues 1198−1235, which exhibit a 100% probability of forming a coiled coil. Exon B (DDK, colored blue) forms an essential part of the binding site for DYNLL2 in MyoVa$^{1194-1316}$ and is located in a region predicted to be unstructured. The binding of DYNLL2 to MyoVa$^{1194-1316}$ stabilizes MyoVa$^{1194-1316}$ against thermal denaturation and causes a structural change in MyoVa$^{1194-1316}$ that is consistent with a gain in its coiled-coil content. On the basis of these findings, we speculate that the second region of putative coiled coil, which spans residues 1246−1275 in MyoVa$^{1194-1316}$ and which exhibits an only 50% probability of forming a coiled coil, assumes the coiled-coil conformation only upon binding DYNLL2.

in Figure 7. We note that dimerization via a predicted coiled-coil domain in the absence of a $[\theta_{222}]/[\theta_{208}]$ ratio typical for the presence of coiled coil has been observed also in the case of the kinesin Kar3p (*60*). Interestingly, the swallow fragment shows a $[\theta_{222}]/[\theta_{208}]$ ratio characteristic of the presence of coiled-coil structure even in the absence of DYNLL2 and under conditions where the fragment is largely monomeric (*36*). In the case of the dynein IC74 intermediate chain fragment, the far-UV CD spectrum indicates a primarily unfolded protein in the absence of DYNLL and a protein with significant α-helical content and possibly coiled-coil structure in the presence of DYNLL (*35*). Thus, the structural effects of binding DYNLL, at least as inferred from far-UV CD spectra, are somewhat different for myosin Va, swallow, and IC74.

Thermal denaturation experiments showed a striking effect of DYNLL2 on the stability of the MyoVa$^{1194-1316}$ fragment in the physiological temperature range. Specifically, the T_m increased from 34.7 °C for MyoVa$^{1194-1316}$ alone to 42.1 °C for the mixture of MyoVa$^{1194-1316}$ and DYNLL2. Because no such change was observed using MyoVa$^{1194-1316}$ΔExonB, which does not bind DYNLL2, and because DYNLL2 itself does not unfold in the observed temperature range, the results with MyoVa$^{1194-1316}$ indicate that its interaction with DYNLL2 dramatically stabilizes its secondary structure.

To further characterize the interaction of DYNLL2 with myosin Va, we determined the affinity of the DYNLL2 dimer for the dimeric MyoVa$^{1194-1316}$ fragment under solution conditions using analytical ultracentrifugation. While the value we obtained ($K_D \sim 0.4$ μM at 4 °C) may differ from the affinity of DYNLL2 for full-length myosin Va, it is similar to the value obtained for the interaction of DYNLL with a fragment of IC74 ($K_D = 0.09 \pm 0.2$ μM) (*35*).

The structural effects exerted by the binding of DYNLL2 on the region of the myosin Va heavy chain surrounding its DYNLL binding site might have significant consequences for the function of native myosin Va given that this myosin exists in an equilibrium between a folded, compact, 14S conformation that is enzymatically and mechanically inactive and an extended 11S conformation that is enzymatically and mechanically active (*39*, *61*−*66*). The transition from the inactive 14S conformation to the active 11S conformation is thought to be induced by the binding of cargo to the myosin's tail domain (*39*, *61*−*66*). A DYNLL-dependent change in the coiled-coil content and/or the stability of the coiled coil in the region of the central stalk domain just N-terminal of the DYNLL2 binding site could affect the ability of myosin Va to assume either conformation, thereby influencing directly the activity of the native molecule. This possibility, together with the likelihood that the binding of myosin Va to DYNLL-interacting proteins like Bmf and GKAP is exon B-dependent, argues that the alternative splicing of this small exon has a significant impact on the function of myosin Va in vivo.

ACKNOWLEDGMENT

We thank Stephen M. King for the gift of anti-DYNLL antibody, Kevin Pfister for the gift of plasmids containing DLC8A and DLC8B, the members of the Hammer lab for useful discussions, Edward D. Korn, James R. Sellers, and Takehito Uruno for a critical reading of the manuscript, and Tom Olszewski for technical assistance.

REFERENCES

1. Reck-Peterson, S. L., Provance, D. W., Jr., Mooseker, M. S., and Mercer, J. A. (2000) Class V myosins, *Biochim. Biophys. Acta 1496*, 36−51.
2. Vale, R. D. (2003) Myosin V motor proteins: Marching stepwise towards a mechanism, *J. Cell Biol. 163*, 445−450.
3. Sellers, J. R., and Veigel, C. (2006) Walking with myosin V, *Curr. Opin. Cell Biol. 18*, 68−73.
4. Cheney, R. E., O'Shea, M. K., Heuser, J. E., Coelho, M. V., Wolenski, J. S., Espreafico, E. M., Forscher, P., Larson, R. E., and Mooseker, M. S. (1993) Brain myosin-V is a two-headed unconventional myosin with motor activity, *Cell 75*, 13−23.
5. Seperack, P. K., Mercer, J. A., Strobel, M. C., Copeland, N. G., and Jenkins, N. A. (1995) Retroviral sequences located within an intron of the dilute gene alter dilute expression in a tissue-specific manner, *EMBO J. 14*, 2326−2332.
6. Wu, X. S., Rao, K., Zhang, H., Wang, F., Sellers, J. R., Matesic, L. E., Copeland, N. G., Jenkins, N. A., and Hammer, J. A., III (2002) Identification of an organelle receptor for myosin-Va, *Nat. Cell Biol. 4*, 271−278.
7. Benashski, S. E., Harrison, A., Patel-King, R. S., and King, S. M. (1997) Dimerization of the highly conserved light chain shared by dynein and myosin V, *J. Biol. Chem. 272*, 20929−20935.
8. Espindola, F. S., Suter, D. M., Partata, L. B., Cao, T., Wolenski, J. S., Cheney, R. E., King, S. M., and Mooseker, M. S. (2000) The light chain composition of chicken brain myosin-Va: Calmodulin, myosin-II essential light chains, and 8-kDa dynein light chain/PIN, *Cell Motil. Cytoskeleton 47*, 269−281.
9. Wang, F., Chen, L., Arcucci, O., Harvey, E. V., Bowers, B., Xu, Y., Hammer, J. A., III, and Sellers, J. R. (2000) Effect of ADP and ionic strength on the kinetic and motile properties of recombinant mouse myosin V, *J. Biol. Chem. 275*, 4329−4335.
10. King, S. M., Barbarese, E., Dillman, J. F., III, Patel-King, R. S., Carson, J. H., and Pfister, K. K. (1996) Brain cytoplasmic and flagellar outer arm dyneins share a highly conserved Mr 8,000 light chain, *J. Biol. Chem. 271*, 19358−19366.
11. King, S. M., and Patel-King, R. S. (1995) The M(r) = 8,000 and 11,000 outer arm dynein light chains from *Chlamydomonas*

flagella have cytoplasmic homologues, *J. Biol. Chem. 270*, 11445−11452.
12. Pfister, K. K., Shah, P. R., Hummerich, H., Russ, A., Cotton, J., Annuar, A. A., King, S. M., and Fisher, E. M. (2006) Genetic Analysis of the Cytoplasmic Dynein Subunit Families, *PLoS Genet. 2*, e1.
13. Wilson, M. J., Salata, M. W., Susalka, S. J., and Pfister, K. K. (2001) Light chains of mammalian cytoplasmic dynein: Identification and characterization of a family of LC8 light chains, *Cell Motil. Cytoskeleton 49*, 229−240.
14. Jaffrey, S. R., and Snyder, S. H. (1996) PIN: An associated protein inhibitor of neuronal nitric oxide synthase, *Science 274*, 774−777.
15. Pfister, K. K., Fisher, E. M., Gibbons, I. R., Hays, T. S., Holzbaur, E. L., McIntosh, J. R., Porter, M. E., Schroer, T. A., Vaughan, K. T., Witman, G. B., King, S. M., and Vallee, R. B. (2005) Cytoplasmic dynein nomenclature, *J. Cell Biol. 171*, 411−413.
16. Naisbitt, S., Valtschanoff, J., Allison, D. W., Sala, C., Kim, E., Craig, A. M., Weinberg, R. J., and Sheng, M. (2000) Interaction of the postsynaptic density-95/guanylate kinase domain-associated protein complex with a light chain of myosin-V and dynein, *J. Neurosci. 20*, 4524−4534.
17. Puthalakath, H., Villunger, A., O'Reilly, L. A., Beaumont, J. G., Coultas, L., Cheney, R. E., Huang, D. C., and Strasser, A. (2001) Bmf: A proapoptotic BH3-only protein regulated by interaction with the myosin V actin motor complex, activated by anoikis, *Science 293*, 1829−1832.
18. Day, C. L., Puthalakath, H., Skea, G., Strasser, A., Barsukov, I., Lian, L. Y., Huang, D. C., and Hinds, M. G. (2004) Localization of dynein light chains 1 and 2 and their pro-apoptotic ligands, *Biochem. J. 377*, 597−605.
19. Fuhrmann, J. C., Kins, S., Rostaing, P., El Far, O., Kirsch, J., Sheng, M., Triller, A., Betz, H., and Kneussel, M. (2002) Gephyrin interacts with dynein light chains 1 and 2, components of motor protein complexes, *J. Neurosci. 22*, 5393−5402.
20. Haraguchi, K., Satoh, K., Yanai, H., Hamada, F., Kawabuchi, M., and Akiyama, T. (2000) The hDLG-associated protein DAP interacts with dynein light chain and neuronal nitric oxide synthase, *Genes Cells 5*, 905−911.
21. Maas, C., Tagnaouti, N., Loebrich, S., Behrend, B., Lappe-Siefke, C., and Kneussel, M. (2006) Neuronal cotransport of glycine receptor and the scaffold protein gephyrin, *J. Cell Biol. 172*, 441−451.
22. Puthalakath, H., Huang, D. C., O'Reilly, L. A., King, S. M., and Strasser, A. (1999) The proapoptotic activity of the Bcl-2 family member Bim is regulated by interaction with the dynein motor complex, *Mol. Cell 3*, 287−296.
23. Schnorrer, F., Bohmann, K., and Nusslein-Volhard, C. (2000) The molecular motor dynein is involved in targeting swallow and bicoid RNA to the anterior pole of *Drosophila* oocytes, *Nat. Cell Biol. 2*, 185−190.
24. Navarro, C., Puthalakath, H., Adams, J. M., Strasser, A., and Lehmann, R. (2004) Egalitarian binds dynein light chain to establish oocyte polarity and maintain oocyte fate, *Nat. Cell Biol. 6*, 427−435.
25. Rodriguez-Crespo, I., Yelamos, B., Roncal, F., Albar, J. P., Ortiz de Montellano, P. R., and Gavilanes, F. (2001) Identification of novel cellular proteins that bind to the LC8 dynein light chain using a pepscan technique, *FEBS Lett. 503*, 135−141.
26. Liang, J., Jaffrey, S. R., Guo, W., Snyder, S. H., and Clardy, J. (1999) Structure of the PIN/LC8 dimer with a bound peptide, *Nat. Struct. Biol. 6*, 735−740.
27. Lo, K. W., Naisbitt, S., Fan, J. S., Sheng, M., and Zhang, M. (2001) The 8-kDa dynein light chain binds to its targets via a conserved (K/R)XTQT motif, *J. Biol. Chem. 276*, 14059−14066.
28. Fan, J., Zhang, Q., Tochio, H., Li, M., and Zhang, M. (2001) Structural basis of diverse sequence-dependent target recognition by the 8 kDa dynein light chain, *J. Mol. Biol. 306*, 97−108.
29. Barbar, E., Kleinman, B., Imhoff, D., Li, M., Hays, T. S., and Hare, M. (2001) Dimerization and folding of LC8, a highly conserved light chain of cytoplasmic dynein, *Biochemistry (Moscow) 40*, 1596−1605.
30. Wang, W., Lo, K. W., Kan, H. M., Fan, J. S., and Zhang, M. (2003) Structure of the monomeric 8-kDa dynein light chain and mechanism of the domain-swapped dimer assembly, *J. Biol. Chem. 278*, 41491−41499.
31. Rodriguez-Crespo, I., Straub, W., Gavilanes, F., and Ortiz de Montellano, P. R. (1998) Binding of dynein light chain (PIN) to neuronal nitric oxide synthase in the absence of inhibition, *Arch. Biochem. Biophys. 359*, 297−304.
32. Fan, J. S., Zhang, Q., Tochio, H., and Zhang, M. (2002) Backbone dynamics of the 8 kDa dynein light chain dimer reveals molecular basis of the protein's functional diversity, *J. Biomol. NMR 23*, 103−114.
33. Lajoix, A. D., Gross, R., Aknin, C., Dietz, S., Granier, C., and Laune, D. (2004) Cellulose membrane supported peptide arrays for deciphering protein-protein interaction sites: The case of PIN, a protein with multiple natural partners, *Mol. Diversity 8*, 281−290.
34. Leopold, P. L., and Pfister, K. K. (2006) Viral strategies for intracellular trafficking: Motors and microtubules, *Traffic 7*, 516−523.
35. Nyarko, A., Hare, M., Hays, T. S., and Barbar, E. (2004) The intermediate chain of cytoplasmic dynein is partially disordered and gains structure upon binding to light-chain LC8, *Biochemistry (Moscow) 43*, 15595−15603.
36. Wang, L., Hare, M., Hays, T. S., and Barbar, E. (2004) Dynein light chain LC8 promotes assembly of the coiled-coil domain of swallow protein, *Biochemistry (Moscow) 43*, 4611−4620.
37. Wu, X., Wang, F., Rao, K., Sellers, J. R., and Hammer, J. A., III (2002) Rab27a is an essential component of melanosome receptor for myosin Va, *Mol. Biol. Cell 13*, 1735−1749.
38. Sheffield, P., Garrard, S., and Derewenda, Z. (1999) Overcoming expression and purification problems of RhoGDI using a family of "parallel" expression vectors, *Protein Expression Purif. 15*, 34−39.
39. Thirumurugan, K., Sakamoto, T., Hammer, J. A., III, Sellers, J. R., and Knight, P. J. (2006) The cargo-binding domain regulates structure and activity of myosin 5, *Nature 442*, 212−215.
40. Zamyatnin, A. A. (1984) Amino acid, peptide, and protein volume in solution, *Annu. Rev. Biophys. Bioeng. 13*, 145−165.
41. Rohl, C. A., and Baldwin, R. L. (1997) Comparison of NH exchange and circular dichroism as techniques for measuring the parameters of the helix-coil transition in peptides, *Biochemistry (Moscow) 36*, 8435−8442.
42. Zolkiewski, M., Redowicz, M. J., Korn, E. D., Hammer, J. A., III, and Ginsburg, A. (1997) Two-state thermal unfolding of a long dimeric coiled-coil: The Acanthamoeba myosin II rod, *Biochemistry (Moscow) 36*, 7876−7883.
43. Lupas, A., Van Dyke, M., and Stock, J. (1991) Predicting coiled coils from protein sequences, *Science 252*, 1162−1164.
44. Berger, B., Wilson, D. B., Wolf, E., Tonchev, T., Milla, M., and Kim, P. S. (1995) Predicting coiled coils by use of pairwise residue correlations, *Proc. Natl. Acad. Sci. U.S.A. 92*, 8259−8263.
45. McDonnell, A. V., Jiang, T., Keating, A. E., and Berger, B. (2006) Paircoil2: Improved prediction of coiled coils from sequence, *Bioinformatics 22*, 356−358.
46. Jones, D. T. (1999) Protein secondary structure prediction based on position-specific scoring matrices, *J. Mol. Biol. 292*, 195−202.
47. Rost, B., Yachdav, G., and Liu, J. (2004) The PredictProtein server, *Nucleic Acids Res. 32*, W321−W326.
48. Muhle-Goll, C., Gibson, T., Schuck, P., Schubert, D., Nalis, D., Nilges, M., and Pastore, A. (1994) The dimerization stability of the HLH-LZ transcription protein family is modulated by the leucine zippers: A CD and NMR study of TFEB and c-Myc, *Biochemistry (Moscow) 33*, 11296−11306.
49. Zhou, N. E., Kay, C. M., and Hodges, R. S. (1994) The role of interhelical ionic interactions in controlling protein folding and stability. De novo designed synthetic two-stranded α-helical coiled-coils, *J. Mol. Biol. 237*, 500−512.
50. Dutta, K., Alexandrov, A., Huang, H., and Pascal, S. M. (2001) pH-induced folding of an apoptotic coiled coil, *Protein Sci. 10*, 2531−2540.
51. Fukuda, M., Kuroda, T. S., and Mikoshiba, K. (2002) Slac2-a/melanophilin, the missing link between Rab27 and myosin Va: Implications of a tripartite protein complex for melanosome transport, *J. Biol. Chem. 277*, 12432−12436.
52. Nagashima, K., Torii, S., Yi, Z., Igarashi, M., Okamoto, K., Takeuchi, T., and Izumi, T. (2002) Melanophilin directly links Rab27a and myosin Va through its distinct coiled-coil regions, *FEBS Lett. 517*, 233−238.
53. Hume, A. N., Collinson, L. M., Hopkins, C. R., Strom, M., Barral, D. C., Bossi, G., Griffiths, G. M., and Seabra, M. C. (2002) The leaden gene product is required with Rab27a to recruit myosin Va to melanosomes in melanocytes, *Traffic 3*, 193−202.

54. Au, J. S., and Huang, J. D. (2002) A tissue-specific exon of myosin Va is responsible for selective cargo binding in melanocytes, *Cell Motil. Cytoskeleton 53*, 89−102.
55. Huang, J. D., Mermall, V., Strobel, M. C., Russell, L. B., Mooseker, M. S., Copeland, N. G., and Jenkins, N. A. (1998) Molecular genetic dissection of mouse unconventional myosin-VA: Tail region mutations, *Genetics 148*, 1963−1972.
56. Westbroek, W., Lambert, J., Bahadoran, P., Busca, R., Herteleer, M. C., Smit, N., Mommaas, M., Ballotti, R., and Naeyaert, J. M. (2003) Interactions of human Myosin Va isoforms, endogenously expressed in human melanocytes, are tightly regulated by the tail domain, *J. Invest. Dermatol. 120*, 465−475.
57. da Silva Bizarioqq, J. C., da Cunha Nascimentoqq, A. A., Casaletti, L., Patussi, E. V., Chociay, M. F., Larson, R. E., and Espreafico, E. M. (2002) Expression of constructs of the neuronal isoform of myosin-Va interferes with the distribution of melanosomes and other vesicles in melanoma cells, *Cell Motil. Cytoskeleton 51*, 57−75.
58. Vadlamudi, R. K., Bagheri-Yarmand, R., Yang, Z., Balasenthil, S., Nguyen, D., Sahin, A. A., den Hollander, P., and Kumar, R. (2004) Dynein light chain 1, a p21-activated kinase 1-interacting substrate, promotes cancerous phenotypes, *Cancer Cell 5*, 575−585.
59. Lei, K., and Davis, R. J. (2003) JNK phosphorylation of Bim-related members of the Bcl2 family induces Bax-dependent apoptosis, *Proc. Natl. Acad. Sci. U.S.A. 100*, 2432−2437.
60. Chu, H. M., Yun, M., Anderson, D. E., Sage, H., Park, H. W., and Endow, S. A. (2005) Kar3 interaction with Cik1 alters motor structure and function, *EMBO J. 24*, 3214−3223.
61. Li, X. D., Jung, H. S., Mabuchi, K., Craig, R., and Ikebe, M. (2006) The globular tail domain of myosin va functions as an inhibitor of the myosin va motor, *J. Biol. Chem.* (in press).
62. Li, X. D., Ikebe, R., and Ikebe, M. (2005) Activation of myosin Va function by melanophilin, a specific docking partner of myosin Va, *J. Biol. Chem. 280*, 17815−17822.
63. Li, X. D., Mabuchi, K., Ikebe, R., and Ikebe, M. (2004) Ca^{2+}-induced activation of ATPase activity of myosin Va is accompanied with a large conformational change, *Biochem. Biophys. Res. Commun. 315*, 538−545.
64. Liu, J., Taylor, D. W., Krementsova, E. B., Trybus, K. M., and Taylor, K. A. (2006) Three-dimensional structure of the myosin V inhibited state by cryoelectron tomography, *Nature* (in press).
65. Krementsov, D. N., Krementsova, E. B., and Trybus, K. M. (2004) Myosin V: Regulation by calcium, calmodulin, and the tail domain, *J. Cell Biol. 164*, 877−886.
66. Wang, F., Thirumurugan, K., Stafford, W. F., Hammer, J. A., III, Knight, P. J., and Sellers, J. R. (2004) Regulated conformation of myosin V, *J. Biol. Chem. 279*, 2333−2336.

BI061142U